ELSEVIER

Biochimica et Biophysica Acta 1370 (1998) 1–7

BIOCHIMICA ET BIOPHYSICA ACTA
BBA

Rapid report

Protein–water–ion interactions in a model of the pore domain of a potassium channel: a simulation study

K.M. Ranatunga, I.D. Kerr, C. Adcock, G.R. Smith, M.S.P. Sansom *

Laboratory of Molecular Biophysics, The Rex Richards Building, University of Oxford, South Parks Road, Oxford OX1 3QU, UK

Received 18 November 1997; accepted 20 November 1997

Abstract

A model of the selectivity filter of a voltage-gated K^+ (Kv) channel formed by an eight-stranded β-barrel is compared with physiological properties of the channel. Continuum electrostatic calculations suggest that only two of the eight Asp sidechains at the extracellular mouth of the pore will ionise. A ring of four Tyr sidechains forms the narrowest region of the pore. Molecular dynamic simulations of the potential energy of a K^+ ion as translated along the model pore indicate that the two ionised Asp sidechains and the hydroxyl groups of the Tyr sidechains stabilise the partially desolvated ion as it passes through the narrowest region. © 1998 Elsevier Science B.V.

Keywords: Ion channel; Potassium channel; Molecular model; Electrostatics; Molecular dynamics

Ion channels play a central role in membrane biophysics, underlying the electrical excitability of cells. Voltage-gated potassium (Kv) channels are important both in their classical role in the depolarising phase of the action potential, and also in the fine-tuning of electrical activity [1]. Kv channels are integral membrane proteins, made up of four identical subunits each of which contains six transmembrane (TM) helices, S1 to S6. The four subunits are packed around a central transbilayer pore. Over the recent years, there has been an enormous increase in our knowledge of the molecular basis of Kv channel function, largely as a result of elegant analyses of site-directed mutagenesis (SDM) and the resultant changes in channel function as measured via patch clamp recording of ionic currents. Such studies have enabled dissection of the relationship between channel function and amino acid sequence [2–5]. In particular, the H5 (or P) loop region, lying between the S5 and S6 TM helices, has been identified as forming the immediate lining of the transbilayer pore, with one H5 loop contributed by each subunit. However, in the absence of a three dimensional crystallographic structure for the Kv protein, it has proved difficult to extend analysis of structure/function relationships to an atomic level. To approach this problem, several investigators have generated molecular models of the Kv-H5 pore domain, using SDM data as guides to and restraints upon possible structures for the pore [6–10]. In a previous paper [9], we combined molecular dynamics (MD) simulations with restraints de-

* Corresponding author. Fax: +44-1865-275182; E-mail: mark@biop.ox.ac.uk

PII S0005-2736(97)00271-X

rived from published SDM data, using a simulated annealing protocol to generate and compare more than 1300 different models of the Kv-H5 domain. In the current paper we examine the predicted functional properties of one of the most plausible models from those generated in the earlier study. In this model (S10839LC in the nomenclature of [9]) the Kv-H5 domain is modelled as an anti-parallel 8-stranded β-barrel. Each H5 loop forms a β-hairpin, with sequence (from the Shaker-A [11] Kv channel): Pro(1′)-*Asp*–Ala–Phe–Trp–Trp–Ala–Val–Val–Thr–Met–Thr–Thr–Val–Gly–*Tyr*–Gly–*Asp*–Met–Thr–Pro(21′) where residues Pro-1′ and Pro-21′ correspond to Pro-430 and Pro-450 respectively in the full length protein. The *highlighted* residues lie at the extracellular mouth (Asp-2′ and Asp-18′) and the midpoint (Tyr-16′) of the pore and play key roles in channel/ion interactions, as will be discussed below. The β-hairpin is folded such that the two ends of H5 (i.e., residues 1′ and 21′) form the extracellular mouth of the pore whilst residues 9′ to 11′ form the intracellular-facing mouth. Thus, residues 1′–8′ form the first strand of the hairpin, the next 3 residues (9′–11′) a loose turn conformation, and the final 9 residues (12′–20′) form the second strand of the hairpin. The overall shear number [12] of the barrel (which determines the pattern of H-bonding between strands) is $S = 10$. The pattern of pore-lining sidechains in this model is in good, if incomplete, agreement with that identified by SDM. Formation of a stable secondary structure (i.e., a β-barrel) by the H5 hairpins is energetically compatible with the pore-forming domain being buried in a relatively hydrophobic environment such as the interior of a membrane protein.

The initial Kv-H5 model was generated by restrained MD simulations in vacuo [9]. In the current study, we describe the predicted functional properties of the model following its refinement by more extended MD simulations with water molecules present within and at either mouth of the Kv-H5 pore. In particular, we examine the likely ionisation states of the rings of Asp-2′ and Asp-18′ sidechains which guard the extracellular mouth of the pore, and analyse the change in potential energy of a K^+ ion as it is translated along the length of the Kv-H5 model pore.

The in vacuo generated Kv-H5 model was solvated with 350 TIP3P [13] water molecules as described in previous papers [14,15]. MD simulations were run using CHARMM [16] v23, with the param19 parameter set, and the H-atoms of apolar groups represented via extended C-atoms. The solvated pore was subjected to 4000 steps of ABNR energy minimization prior to MD simulations. During the MD simulations, intra-loop and inter-loop distance restraints were used to maintain the H-bonding pattern of the β-barrel. A cylindrical restraining potential [14] was employed to prevent evaporation of water molecules from the caps of waters at the mouths of the pore. The Kv-H5 model was oriented such that its pore axis was coincident with the z axis, with the pore mouths at $z = -15$ Å (intracellular) and $z = +15$ Å (extracellular). The two rings of Asp residues guarding the extracellular mouth were located at z = ca. $+5$–$+10$ Å (see Fig. 1). In this first simulation, all eight Asp sidechains were assumed to be in their fully ionized (i.e., $-CO_2^-$) state. Simulations were for 250 ps at 300 K, after 9 ps heating and 6 ps equilibration periods [14,15]. A 1 fs timestep was used, with SHAKE to fix X–H bond distances.

The pore geometry was monitored during the course of the simulation, using the program HOLE [17,18] to determine pore radius profiles from snapshots of the structure taken every 1 ps. The time-

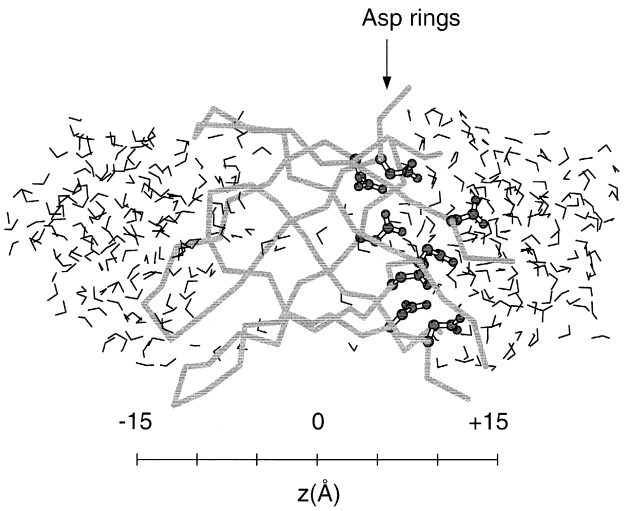

Fig. 1. Kv–H5 pore model plus water molecules, showing a snapshot of the pore model from a MD trajectory. The Ca trace is depicted using thick grey lines, with the two rings of acidic (Asp-2′ and Asp-18′) sidechains in ball-and-stick format. The water molecules are shown as 〈 shapes. The pore axis runs from ca. $z = -15$–$+15$ Å, and negative z values correspond to the intracellular mouth of the pore.

averaged minimum radius of the pore was 0.75 ($\pm$0.13) Å, i.e., somewhat less that the ionic radius of K^+ (1.3 Å). However, this radius fluctuated dynamically, at times reaching 1.34 Å. Interestingly, the minimum radius of the pore was in the vicinity of the ring of Tyr-16′ sidechains. The Gly–Tyr–Gly motif of the H5 sequence has been shown to be a fingerprint for K^+ selectivity in sequences of Kv and related channels [19,20]. From a pore radius profile, one may obtain an approximate prediction of the pore conductance, by integration of the ohmic resistance along the length of the pore and application of an empirical scale factor based on analysis of channels for which both atomic resolution structures and ionic conductance data are available [18]. This yields a time-averaged predicted conductance of 5.4 ($\pm$1.9) pS for the Kv-H5 model (in 100 m KCl), at times fluctuating to ca. 8 pS. This is a little lower than the corresponding experimental measurement (ca. 19 pS [21,22]), but is within the expected accuracy of this (necessarily approximate) method of conductance prediction. Thus, both the geometry of the pore and the nature of the sidechains lining its narrowest region are broadly consistent with available experimental data.

The structure and dynamics of water molecules within and at either mouth of the pore were examined (Table 1), revealing similar patterns to those observed both in simplified models of pores formed by β-barrels [14,23] and in models of channels formed by bundles of parallel α-helices [14,24]. In this analysis, the system was divided into four zones: the internal mouth of the pore; the external mouth of the pore; an outer pore adjacent to each mouth (treated together as one ‘vestibule’ zone) and an inner pore. The translational mobility of the water molecules (D) within the inner pore was highly restricted, both relative to the caps at either mouth of the pore and to simulations of bulk TIP3P water [14]. Similarly, the rotational motion ($1/\tau$) of the inner pore waters was highly restricted, although in this case the contrast with the waters in the mouths is less marked as the ring of negatively charged sidechains at the external mouth also hinder water rotational motions. Water within the inner pore per se formed a nearly single-file column, about 9 water molecules long. These waters were oriented such that their oxygen atoms were directed towards the intracellular mouth of the pore. This orientation, reflected in the projection of their dipoles onto the pore axis ($\mu_z = +1.28$ Debye; see Table 1), results from their electrostatic interactions with the ring of acidic sidechains at the extracellular mouth of the pore. Thus, within the narrowest region of the pore, the water molecules are oriented and relatively immobile.

The rings of Asp-2′ and Asp-18′ residues were anticipated to play a role in pore/ion interactions. However, the question of what the ionisation states of these sidechains are within the pore, as they are in close proximity to one another and are located at the interface between a low dielectric (protein) and high dielectric (water) environment arises. In order to estimate the pK_As of these Asp sidechains, in situ standard methods via numerical solution of the Poisson–Boltzmann equation were employed, using the program UHBD [25]. We note that similar methods have been applied with some success to the acidic and basic sidechains which form the narrowest region

Table 1
Water properties

Zone	Internal cap	Outer pore (‘vestibules’)	Inner pore (‘selectivity filter’)	External cap
N	ca. 101	ca. 168	ca. 9	ca. 70
D (Å^2 ps^{-1})	0.17 ($\pm$0.05)	0.09 ($\pm$0.06)	0.02 ($\pm$0.02)	0.21 ($\pm$0.07)
$1/\tau$ (ps^{-1})	0.16 ($\pm$0.09)	0.05 ($\pm$0.04)	0.01 ($\pm$0.01)	0.05 ($\pm$0.04)
μ_z (Debye)	$-$0.05 ($\pm$1.48)	$-$0.49 ($\pm$1.43)	+1.28 ($\pm$1.06)	$-$0.74 ($\pm$1.35)

Zones: The internal and external caps refer to those waters at the respective mouths of the pore model. The outer pore (‘vestibule’) refers to those water in the two outer regions of the pore, between the caps and the narrowest region (the inner pore). With reference to Fig. 1, water is classified as in: the internal cap if $z < -15$ Å; the outer pore if -15 Å $< z < -6$ Å or if $+6$ Å $< z < +17$ Å; the inner pore if -6 Å $< z < +6$ Å; or the external cap if $+17$ Å $< z$. N is the number of water molecules in a zone; D is the self diffusion coefficient; $1/\tau$ is the rotational reorientation rates; and μ_z is the projection of the water molecule dipole onto the pore (i.e., z) axis. All values are given as mean ($\pm$S.D.) for all water molecules in a zone.

of the pore in bacterial porins [26] and to the ionizable groups within bacteriorhodopsin [27]. The Kv–H5 model was embedded in a low dielectric ($\epsilon = 4$) slab in order to mimic the presence of the surrounding transmembrane regions of the protein and of the lipid bilayer. Solvent, both outside and within the pore, was modelled as a dielectric of 78, with an ionic strength of 100 mM. Titration curves were calculated [28] for all ionizable residues within the model via a two-stage procedure for each residue. Firstly, the intrinsic pK_A, reflecting the effect of the local dielectric environment, was calculated, by assuming that all ionizable residues of the protein other than the one in question were in their electrically neutral state. Secondly, the effect of each residue's interaction with all other ionizable groups in the protein was determined for all possible combinations of ionisation state. To take into account the effects of dynamic fluctuations in structure, pK_As were estimated for four snapshot structures (at $t = 15.5$, 115.5, 215.5 and 265 ps) from the MD trajectory.

The Asp residues fall into three groups on the basis of their predicted titration behaviour. Thus, the Asp-2′ residues exhibit a mean pK_A of 14.8 (± 4.6), i.e., considerably higher than the value of 4.0 for an isolated Asp sidechain. This appears to be due to the unfavourable electrostatic interactions between adjacent Asp-2′ residues when ionized, and also the location of these sidechains close to the surrounding low dielectric region which represents the remainder of the channel protein and the bilayer. Thus, at pH 7 the Asp-2′ sidechains have an average probability of ionization of only 0.07. The Asp-18′ residues exhibit more complex behaviour (Fig. 2). As the pH is raised from 0 to 7, two Asp-18′ sidechains (which are located on opposite sides of the pore from one another) ionize, whilst the other two Asp-18′ sidechains remain protonated. As the pH is raised above 7, a switch in which pair of Asp-18′ sidechains is protonated may occur, depending on which snapshot of the structure is considered. Averaging over the four snapshots, at pH 7, two Asp-18′ residues have a probability of ionization of ca. 0.5, whereas two have a probability of ionization of ca. 0.3. For the final ($t = 265$ ps) snapshot, two Asp-18′ sidechains have a probability of ionization of ca. 0.9, whereas the other two are fully protonated. Such complex titration behaviour is not merely a theoretical nicety, but has been observed, e.g., in NMR studies of diethylenetriaminepentaacetic acid (DPTA), a metal-ion chelating agent in which the covalent structure brings five carboxylate groups into close proximity [29]. In the context of the physiological properties of Kv channels, these calculations suggest that at neutral pH the Asp-2′ sidechains and two of the Asp-18′ sidechains will remain protonated. Although the pK_A values estimated for the Asp-2′ and for two of the Asp-18′ sidechains are probably a little unreliable, they clearly indicate that these sidechains have high pK_A values and so remain protonated. Thus, the most likely state of the H5–Kv model pore is one in which only an opposing pair of Asp-2′ sidechains are ionized.

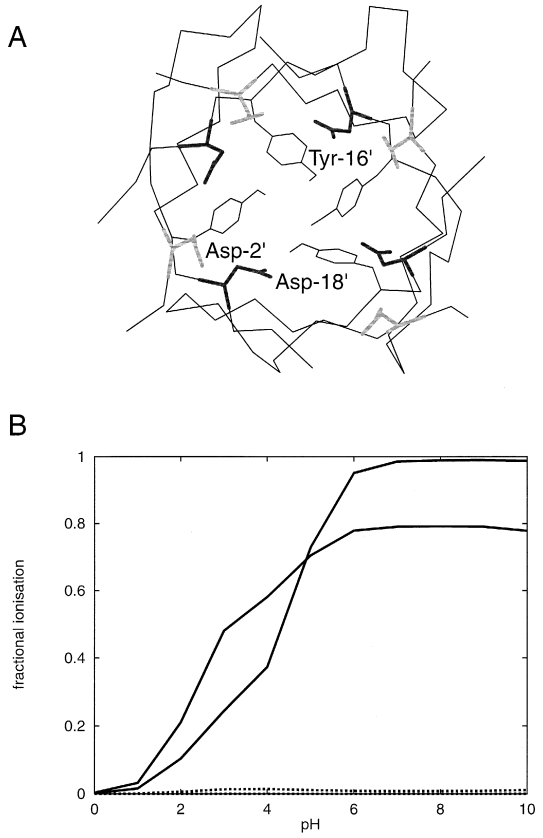

Fig. 2. Titration of Asp sidechains which form the extracellular mouth of the pore. (A) Ca-trace of the pore viewed down the pore axis, with the Asp-2′ (thick pale grey lines), Tyr-16′ (thin black lines) and Asp-18′ (thick dark grey lines) sidechains. (B) Titration curves calculated from a single snapshot of the pore structure from the MD trajectory. Two Asp-18′ residues (solid lines) titrate with an average pK_A of 3.6, whereas the other two Asp-18′ residues (broken lines) titrate with pK_As of > 15.

A further consideration was the possibility of deprotonation of one or more Tyr-16′ sidechains. To explore this, the pK_A calculations were repeated whilst allowing for the possibility of ionisation of tyrosine sidechains. In none of the four structures was a Tyr sidechain ionised at pH 7.0. Thus, under physiological conditions, it seems that the Tyr-16′ ring remains fully protonated. Thus, the most likely configuration of the system remains is one in which only two Asp-18′ sidechains form a negatively charged pair at the extracellular mouth of the pore.

To explore the consequences of this difference from the 'standard' ionisation state of the Asp residues, a further 250 ps MD simulation of the Kv–H5 model was performed in which the four Asp-2′ and two of the Asp-18′ sidechains were protonated. This yielded a time-averaged minimum radius of 0.36 ($\pm$0.18) Å (with fluctuations up to 1.07 Å) and a corresponding average predicted conductance of 4.0 ($\pm$1.8) pS, with fluctuations up to 8.4 pS. Thus, the maximum value of the predicted conductance during this simulation is also a little lower than that observed experimentally.

The consequences of this model in terms of ion/protein/water interaction energies were explored by a series of short MD simulations in which a single K^+ ion was translated along the length of the model Kv–H5 pore, using a similar procedure to that used to explore ion/protein/water energetics in a model of the pore domain on the nicotinic acetylcholine receptor [30]. The starting point for these simulations were snapshots from the previous simulations in which the water but not the ion were present. A K^+ ion was placed at successive positions along the z axis, separated by 1 Å steps. For each position of the ion, the nearest water molecule was removed, the system was energy minimised (3000 steps of ABNR), and then a short burst (6 ps of heating to 300 K followed by 9 ps of equilibration) of MD was performed. The energetics of ion/protein, ion/water and ion/protein/water interactions were averaged over the final 9 ps of the 15 ps run for each position of the ion. The results of these simulations are presented in terms of potential energy profiles for ion/(water + protein) (Fig. 3A), ion/protein and ion/water interactions (Fig. 3B). Three sets of simulations were performed: (i) with all eight Asp sidechains (i.e., 4 Asp-2′ and 4 Asp-18′) ionised; (ii) with all eight Asp sidechains protonated; and (iii) with just two Asp-18′ sidechains ionised. The assumed ionisation state has a significant quantitative effect on the overall potential energy profile of the ion. With eight Asp residues ionised, there is a potential energy well for the cation of depth ca. -100 kcal/mol (i.e., ca. 170 RT), in the vicinity of the Asp rings. Once within such a well, a K^+ ion would be unlikely to escape. Thus, this configuration of the system would not be compatible with a high channel conductance (NB. 19 pS at 100 mV = 1.2×10^7 ions/s). If, in the light of the pK_A calculations, only two Asp-18 sidechains are assumed to be ionised the well depth is reduced to ca. -20 kcal/mol. Indeed, there is also in this case a barrier to ion permeation in the narrowest region of the channel (ca. $z = 0$ Å). The deepest region of the well is at $z = +10$ Å, i.e., in the extracellular mouth of the pore, a region where other residues, contributed by the pre-H5 and post-H5 vestibule regions of the Kv protein, might influence the potential energy of the ion. In contrast, if one assumes that all eight Asp sidechains are protonated then there is no longer a potential well and the barrier height is increased to ca. 60 kcal/mol. Thus, the ionisation of just two Asp sidechains seems to be compatible with a cation permeable pore.

It is informative to examine the energetics of ion permeation in a little more detail. If the overall interaction potential profile of the ion is broken down into its constituent terms, a common pattern emerges (Fig. 3B). Thus, the well in the ion/protein interaction energy is mirrored by a barrier in the ion/water interaction energy profile. This suggests that as the ion enters the narrowest region of the pore, it is (partially) dehydrated. Favourable interactions with the pore-lining sidechains to some extent outweigh the energetic costs of such desolvation, the final balance depending on the ionisation state of the sidechains. Of course, it should be remembered that these profiles are of potential energies rather than free energies, but even so they provide an insight into the interactions of the ion with the pore. Investigation of the contribution of the individual sidechains (Fig. 3C) to the well in the ion/protein interaction profile reveals the major contributions are from: (i) the Asp-18′ ring which generates a well of depth ca. -140 kcal/mol at $z = +6$ Å (i.e., at the extracellu-

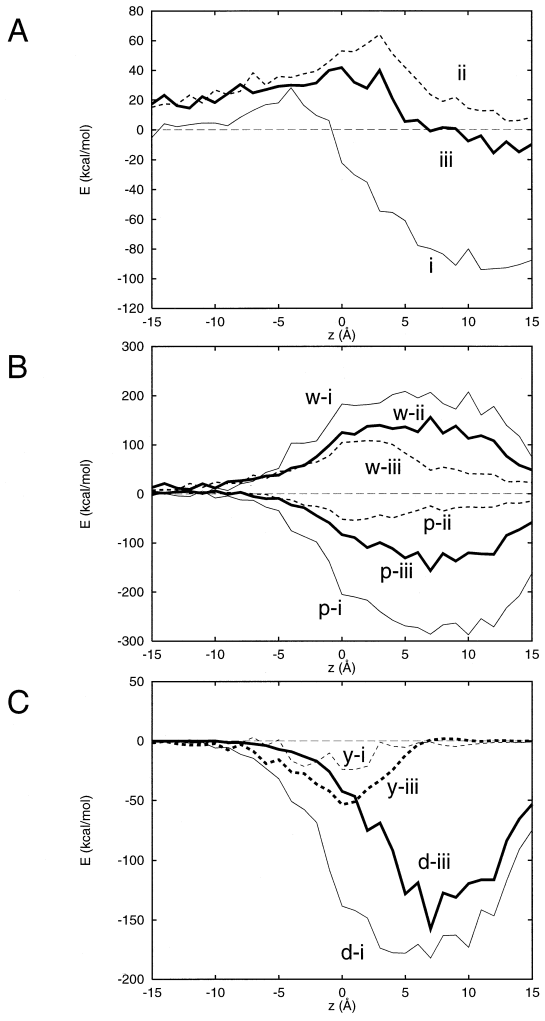

Fig. 3. Interaction energy profiles for translation of a K^+ ion along the solvated Kv–H5 pore model: (A) Potential energy of interaction of the ion with (pore + water) as a function of distance along the pore (z) axis; (B) Interaction energy of the ion with water (upper curves) and with the pore (lower curves); and (C) Interaction energy of the ion with the Tyr-16′ (broken curves) and Asp-2′ (solid curves) sidechains. In graphs (A) and (B), profiles are shown for all three sets of simulations, i.e.: (i) thin solid lines—with all eight Asp sidechains (i.e., 4 Asp-2′ and 4 Asp-18′) ionised; (ii) broken lines—with all eight Asp sidechains protonated; and (iii) thick solid lines—with just two Asp-18′ sidechains ionised. In (C), profiles are shown only for simulations ((i) thin lines) and ((iii) thick lines).

lar mouth of the pore); and (ii) the ring of Tyr-16′ sidechains, which yields a well of depth from ca. −50 kcal/mol at z ca. 0 Å (i.e., midway along the pore). Thus, in this model of the Kv–H5 pore the Tyr-16′ sidechain ring both forms the narrowest region of the pore and interacts favourably with a K^+ ion as it passes through the pore in its desolvated state. This correlates nicely with experimental evidence in favour of this Tyr residue playing a role in governing the cation selectivity of the channel [19]. In evaluating the significance of these results, it should be remembered that the simulations are based upon a model structure for the H5 pore-forming domain of a Kv channel. Therefore, it is likely that details may differ between the model structure and an (as yet undetermined) experimental structure. However, this model represents a current ‘best guess’ at the architecture of the Kv–H5 pore. Furthermore, transmembrane segments outside of H5 have not been included in this model. Although they are not thought to contribute directly to the pore lining, they may well modulate the structural and electrostatic properties of the pore at either or both mouths.

Despite these limitations, analysis of this model highlights some general problems which will need to be addressed for Kv channels. In particular, it is evident that especial attention will need to be paid to the ionisation states of the rings of Asp sidechains which are believed to lie at the extracellular mouth of the pore. In our simulations, we have considered a number of limiting cases in which certain sidechains are assumed to be either fully ionised or fully protonated during passage of a K^+ ion. The true situation may be rather more complex. It is likely that the presence of a cation within such a pore may in itself change the probability of ionisation of a sidechain. Furthermore, dynamic fluctuations in the pore structure may result in fluctuations in sidechain pK_As, as has been observed in recent simulation and electrostatics studies of bacteriorhodopsin [31]. These, and other complexities (e.g., multi-ion occupancy of the pore) will need to be addressed in future simulations.

This work was supported by grants from the Wellcome Trust. Our thanks to the Oxford Centre for Molecular Sciences for access to computer facilities.

References

[1] B. Hille, Ionic Channels of Excitable Membranes, 2nd edn., Sinauer Associates, Sunderland, MA, 1992.
[2] C. Miller, Science 252 (1991) 1092–1096.
[3] O. Pongs, J. Membr. Biol. 136 (1993) 1–8.

[4] A.M. Brown, Annu. Rev. Biophys. Biomol. Struct. 22 (1993) 173–198.
[5] Q. Lü, C. Miller, Science 268 (1995) 304–307.
[6] S. Bogusz, A. Boxer, D.D. Busath, Protein Eng. 5 (1992) 285–293.
[7] J.C. Bradley, W.G. Richards, Protein Eng. 7 (1994) 859–862.
[8] S.R. Durell, H.R. Guy, Neuropharmacology 35 (1996) 761–773.
[9] I.D. Kerr, M.S.P. Sansom, Biophys. J. 73 (1997) 581–602.
[10] P.K. Yang, C.Y. Lee, M.J. Hwang, Biophys. J. 72 (1997) 2479–2489.
[11] B.L. Tempel, D.M. Papazian, T.L. Schwarz, Y.N. Jan, L.Y. Jan, Science 237 (1987) 770–775.
[12] A.G. Murzin, A.M. Lesk, C. Chothia, J. Mol. Biol. 236 (1994) 1369–1381.
[13] W.L. Jorgensen, J. Chandresekhar, J.D. Madura, R.W. Impey, M.L. Klein, J. Chem. Phys. 79 (1983) 926–935.
[14] J. Breed, R. Sankararamakrishnan, I.D. Kerr, M.S.P. Sansom, Biophys. J. 70 (1996) 1643–1661.
[15] P. Mitton, M.S.P. Sansom, Eur. Biophys. J. 25 (1996) 139–150.
[16] B.R. Brooks, R.E. Bruccoleri, B.D. Olafson, D.J. States, S. Swaminathan, M. Karplus, J. Comp. Chem. 4 (1983) 187–217.
[17] O.S. Smart, J.M. Goodfellow, B.A. Wallace, Biophys. J. 65 (1993) 2455–2460.
[18] O.S. Smart, J. Breed, G.R. Smith, M.S.P. Sansom, Biophys. J. 72 (1997) 1109–1126.
[19] L. Heginbotham, Z. Lu, T. Abramsom, R. MacKinnon, Biophys. J. 66 (1994) 1061–1067.
[20] I.D. Kerr, M.S.P. Sansom, Nature 373 (1995) 112.
[21] L. Heginbotham, R. MacKinnon, Biophys. J. 65 (1993) 2089–2096.
[22] M. Tagliatela, M.S. Champagne, J.A. Drewe, A.M. Brown, J. Biol. Chem. 269 (1994) 13867–13873.
[23] M.S.P. Sansom, I.D. Kerr, Biophys. J. 69 (1995) 1334–1343.
[24] I.D. Kerr, R. Sankararamakrishnan, O.S. Smart, M.S.P. Sansom, Biophys. J. 67 (1994) 1501–1515.
[25] M.E. Davis, J.D. Madura, B.A. Luty, J.A. McCammon, Comput. Phys. Commun. 62 (1991) 187–197.
[26] A. Karshikoff, V. Spassov, S.W. Cowan, R. Ladenstein, T. Schirmer, J. Mol. Biol. 240 (1994) 372–384.
[27] D. Bashford, K. Gerwert, J. Mol. Biol. 224 (1992) 473–486.
[28] D. Bashford, M. Karplus, J. Phys. Chem. 95 (1991) 9556–9561.
[29] J.L. Sudmeier, C.N. Reilley, Anal. Chem. 36 (1964) 1699–1706.
[30] G.R. Smith, M.S.P. Sansom, Biophys. J. 73 (1997) 1364–1381.
[31] L. Sandberg, O. Edholm, Biophys. Chem. 65 (1997) 189–204.